Memoirs of the Faculty of Engineering, Okayama University, Vol.25, No. 2, pp.39-54, March 1991

Prediction of Transient and Steady Turbulent Free Subsonic Air Jets

Felix Chintu NSUNGE*, Eiji TOMITA**
and Yoshisuke HAMAMOTO**

(Received February 18, 1991)

SYNOPSIS

Velocity distributions and related parameters of transient and steady, turbulent air jets issuing under atmospheric conditions at Mach 0.14, 0.33 and 0.5 have been predicted using Navier-Stokes(N-S) equations for compressible flow and incompressible flow independently with the k-ε model. The closeness and consistence of the results predicted by the N-S equations for compressible and incompressible flows as well as with relevant measurement or similar prediction show that the incompressible flow assumption for at least some subsonic gas jets issuing at velocities higher than Mach 0.3, the general limit for incompressible fluid flow, can be reasonably accurate particularly in the main fully developed flow region. This suggests that the divergence term in source terms of the momentum, turbulence energy and its dissipation rate equations have negligible effects for some seemingly compressible high speed, subsonic free gas jets. The computation time is reduced by at least 18 % when incompressible flow assumption is used.

1. INTRODUCTION

Experimental results from many sources[1] have shown that trends of velocity and temperature distributions in incompressible and compressible free gas jets are identical. This empirical fact has led some researchers notably Abramovich[1], Pai[2], Kumar[3] to suggest

* Graduate School of Natural Science and Technology
** Dept. of Mechanical Engineering

that at least for engineering purposes, some high speed, subsonic free gas jets may be assumed to be incompressible not only in the inviscid potential core where the observed velocities, pressure, temperature and so density are constant, but also outside the potential core and particularly in the fully developed main region where flow velocities are low at less than about Mach 0.63 for say the extreme case of the sonic gas jet. For instance, for the fastest air jet at Mach 0.5 investigated here, the maximum Mach number in the main region as estimated from semi-empirical velocity decay laws is about 0.32 while the maximum density variation is about 4 %. Generally in fluid flow, low speed gas flow at velocities below Mach 0.3 is treated as incompressible flow because density variation is negligible[2-4]. Other criteria that may be used for identifying incompressible flow is the maximum density variation in the flow which some researchers set at up to 10 %. Whichever criteria is used, the main implication of incompressible flow as applies to equations governing continuum fluid flow particularly the continuity and Navier-Stokes equations as well as the turbulence energy dissipation rate equation when eddy viscosity is estimated by the high version of the two-equation k-ε turbulence model is that the constant density causes the divergence in the continuity equation to vanish and consequently the same divergence term in the source terms of the momentum, turbulence energy and its dissipation rate equations equally disappear from these equations and only the velocities, pressure and in addition temperature need to be solved for non-isothermal flows. Since even in cold incompressible fluid flows small variations in temperature do exist in order to offset the pressure variations so as to maintain constant density, temperature here may be solved or assumed to be constant. Here particularly because of the need to approximate all initial variable fields, this being inherent in numerical iteration methods which the simple algorithm also uses due to non-linearity of the governing equations, velocity, pressure and temperature fields have been calculated.

The problems solved involve two kinds of single shot, turbulent free air jets issuing at an initial velocity, Uo under atmospheric conditions of the surrounding air. The transient jet is characterised by a short air injection time period of 10 ms while the steady jet is one in which injection continues for a much longer time to allow the jet to develop to its steady state. Both types of jets are injected from a small 1 mm diameter automobile injector orifice.

Similar gas jets find applications in many fluid mixing systems like diffusion combustion furnaces and internal combustion engines, thrust force propulsion systems like rocket, gas turbine jet engines, helicopter engines for vertical take off and landing as well as in fluid mixers.

2. GOVERNING EQUATIONS

2.1 Compressible flow

The governing equations used in the compressible flow solution approach are the complete N-S equations represented by the general property transport equation used in prediction of methane free gas jet[5] for all variables except the species mass fraction because in the present study, the injected and surrounding gases are identical.

2.2 Incompressible flow

The equations used in the incompressible flow solution take the following form after divergence terms, $\nabla.\bar{U}$, are removed from source terms of momentum, turbulence energy and its dissipation rate equations since the density is now assumed to be constant. Definitions of variables and other related symbols remain the same as given in[5]

$$\rho\frac{\partial}{\partial t}(\phi) + \rho\frac{\partial}{\partial x}(u\phi) + \rho\frac{1\partial}{r\partial r}(rv\phi) = \frac{\partial}{\partial x}(\Gamma_\phi\frac{\partial\phi}{\partial x}) + \frac{1\partial}{r\partial r}(r\Gamma_\phi\frac{\partial\phi}{\partial r}) + S_\phi \qquad (1)$$

where t, ρ, r and x stand for time, density, axial and radial coordinates, Γ_ϕ, S_ϕ are corresponding effective diffusivity and variable source term whose definitions are given in Table.1.

Table.1 Definitions of coefficients and source terms in Eq.(1)

ϕ	Γ_ϕ	Source term, S_ϕ
1	0	S'_ρ
u	μ_e	$\frac{\partial}{\partial x}(\mu_e\frac{\partial u}{\partial x}) + \frac{1\partial}{r\partial r}(r\mu_e\frac{\partial v}{\partial r}) - \frac{\partial p}{\partial x} - \frac{2\partial}{3\partial x}(\rho k) + S'_u$
v	μ_e	$\frac{\partial}{\partial x}(\mu_e\frac{\partial u}{\partial r}) + \frac{1\partial}{r\partial r}(r\mu_e\frac{\partial v}{\partial r}) - \mu_e\frac{v}{r^2} - \frac{\partial p}{\partial r} - \frac{2\partial}{3\partial r}(\rho k) + S'_v$
h	$\frac{\mu_e}{\sigma_h}$	$\frac{\partial p}{\partial t} + \frac{\partial}{\partial x}\{\mu_e(1-\frac{1}{\sigma_h})\frac{\partial}{\partial x}(\frac{u^2}{2}+\frac{v^2}{2})\} + \frac{1}{r}\frac{\partial}{\partial r}\{r\mu_e(1-\frac{1}{\sigma_h})\frac{\partial}{\partial r}(\frac{u^2}{2}+\frac{v^2}{2})\} + \frac{\partial}{\partial x}\{\mu_e(\frac{1}{\sigma_k}-\frac{1}{\sigma_h})\frac{\partial k}{\partial x}\} + \frac{1\partial}{r\partial r}\{r\mu_e(\frac{1}{\sigma_k}-\frac{1}{\sigma_h})\frac{\partial k}{\partial r}\} + S'_h$
k	$\frac{\mu_e}{\sigma_k}$	$G - \rho\varepsilon + S'_k$
ε	$\frac{\mu_e}{\sigma_\varepsilon}$	$\frac{\varepsilon}{k}(C_1 G - C_2\rho\varepsilon) + S'_\varepsilon$

Here, $G = \mu_e\{2((\frac{\partial u}{\partial x})^2 + (\frac{\partial v}{\partial r})^2) + (\frac{\partial u}{\partial r} + \frac{\partial v}{\partial x})^2 + 2(\frac{v}{r})^2\}$

The k-ε turbulence model constants C_μ, C_1, C_2, σ_k, σ_ε used are 0.09, 1.44, 1.92, 1.0, 1.3 respectively while the effective Prandtl number, σ_h is 0.7. The dynamic eddy viscosity, μ_t is calculated from the semi-empirical relation[6,7];

$$\mu_t = C_\mu \rho k^2/\varepsilon$$

2.3 Auxillary relations

In both compressible and incompressible flow solutions, Sutherland's law[4] has been used to evaluate molecular viscosity which varies with temperature. The ideal gas equation has been used to calculate densities only in the case of compressible flow solution approach because the density is non-uniform for this case. These auxillary relations close the two systems of equations solved independently for the compressible and incompressible solution approaches. Each system of equations is solved simultaneously in an iteration scheme identical to that used in ref.5.

2.4 Boundary and initial conditions

Boundary conditions in both incompressible and compressible flow solution approaches are essentially identical to those used for the solution of the methane gas jet[5] with the species mass fraction equation and its boundary conditions removed because the species mass fraction is not solved for in the present air jet calculations. For instance to simulate free jet conditions the temperature and density of the surrounding room air were again set at 301.15 K and 1.18 kg/m^3 respectively in both solution approaches. Initial velocities, Uo used for the three independent cases studied were 45, 105 and 160 m/s while the initial exit radial velocities Vo were set to zero. Initial densities, ρ_o and temperatures, To also set uniform across the nozzle opening were estimated from the ideal gas and isentropic law[3] with the effective injection to surrounding air pressure ratio obtained through the energy balance formula are given in Table 2. Initial conditions for turbulence energy and its

Table 2 Initial conditions at nozzle exit

U_o m/s	V_o m/s	T_o K	ρ_o kg/m^3
45	0	300.14	1.9
105	0	295.7	1.194
160	0	288.4	1.228

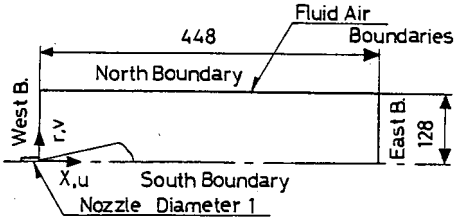

Fig.1 Calculation domain

dissipation rate being functions of the initial velocity, Uo were set as defined in the solution of the methane gas jet[5].

2.5 Numerical procedure

Using control volume formulation, Eq.(1) is discretized into a general finite difference equation and the SIMPLE algorithm[8] is applied on the calculation domain shown in Fig.1. As outlined in the solution of the methane gas jet[5] again the pressure fields are first guessed and tentative velocity u, v fields and subsequently other variable fields are calculated. Their accuracy is checked in the continuity equation before correction, if necessary, is made to the pressure fields. This is repeated in an iteration procedure until the pre-set convergence condition like the sum of mass efflux in all control volumes or the velocity difference between adjacent iterations and timesteps at suitable convergence monitoring points is practically zero for transient and steady jet flow conditions respectively.

3. RESULTS

3.1 Numerical performance

Although coarser computational grids like 21x31, 41x31 for grid nodes in the axial and radial directions as well as smaller and bigger timesteps like 0.1, 1 ms were tried with reasonably good results, a 51x41 computational grid using timesteps 0.2 and 0.5 ms for transient and quasi-steady jets respectively were finally found to be accurate enough and used in all results here. Because the injector orifice is small, finite space lengths were stretched at rates of 1.07 and 1.21 in the axial and radial directions respectively.

The iteration convergence was set to be attained when the net flow on the whole grid was practically zero or the change in axial

velocity, u at a suitable grid node on the jet axis was less than 0.003 m/s between adjacent iterations within the same timestep. The total calculation time periods for transient and quasi-steady jets were 20 and 247 ms respectively. With the number of iterations per timestep varying from 30 to 110 to attain convergence for the incompressible flow solutions, a total of about 7000 and 34580 iterations were executed in each complete run for transient and quasi-steady jets respectively on the ordinary NEC-ACOS2010 Computer. However using the same 51x41 grid, the total computer CPU time, varied with the jet initial velocity, Uo and varied from 200 to 400 sec for transient jets and 300 to 631 sec for quasi-steady jets for the incompressible flow solutions. These CPU times were at least 18 % lower than those used in the compressible flow solutions for the jets with the same initial velocity.

3.2 Calculated results

Some results of the two prediction approaches which involve independent application of firstly N-S and k-ε property transport equations for compressible fluid flow and secondly those for compressible fluid flow to solve the same air jet flow problems are presented here mainly for the typical case of the fastest jet with initial velocity, Uo =160 m/s. However, although all predicted results for jets at initial velocity, Uo =45 and 105 m/s are not presented here, the predicted global trends of their velocity distributions and other related parameters closely for the jet at Uo =160 m/s presented here.

Figure 2 shows typical distributions of transient mean axial velocity as predicted independently by the compressible and incompressible flow solution approaches at several locations on the jet axis for the air jet with initial velocity, Uo =160 m/s. At each location near the injector, the velocity rises to a maximum steady value with the rate of rise decreasing with the axial distance, x from the nozzle while at locations far from the injector maximum steady values are not attained by the time the air injection is stopped at 10 ms. After air injection is stopped, velocities decrease towards zero with the rate of fall decreasing with the axial distance in a similar way exhibited during their rise. Although there are some discrepancies especially in the transition region of the jet, the compressible and incompressible flow solutions seem essentially the same. Moreover, these predicted trends of the velocity distributions compare

reasonably well with experimental data obtained by other researchers like Witze[9] for similar transient jets issuing from small round orifices.

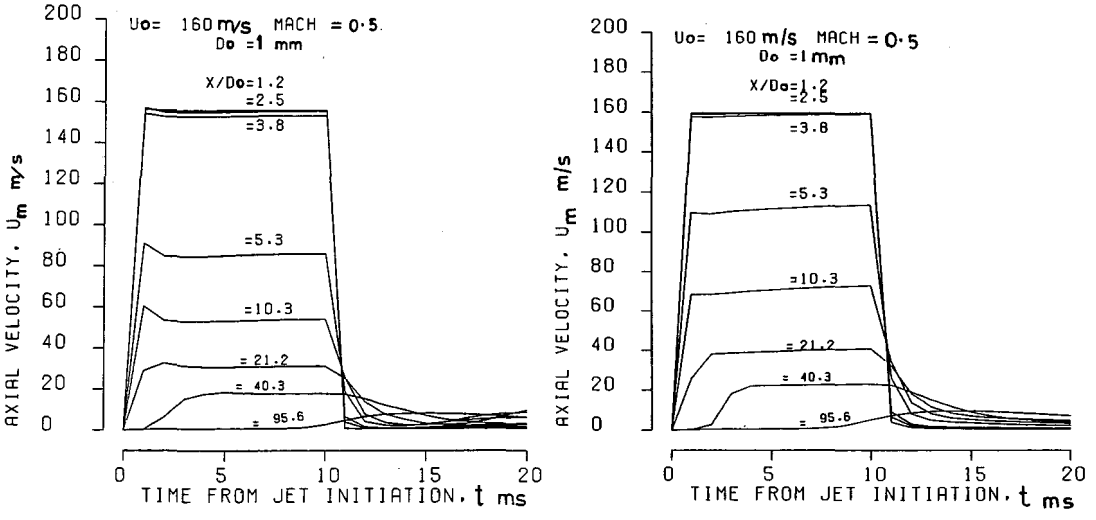

(a) Compressible (b) Incompressible

Fig.2 Histories of mean axial velocities on jet axis

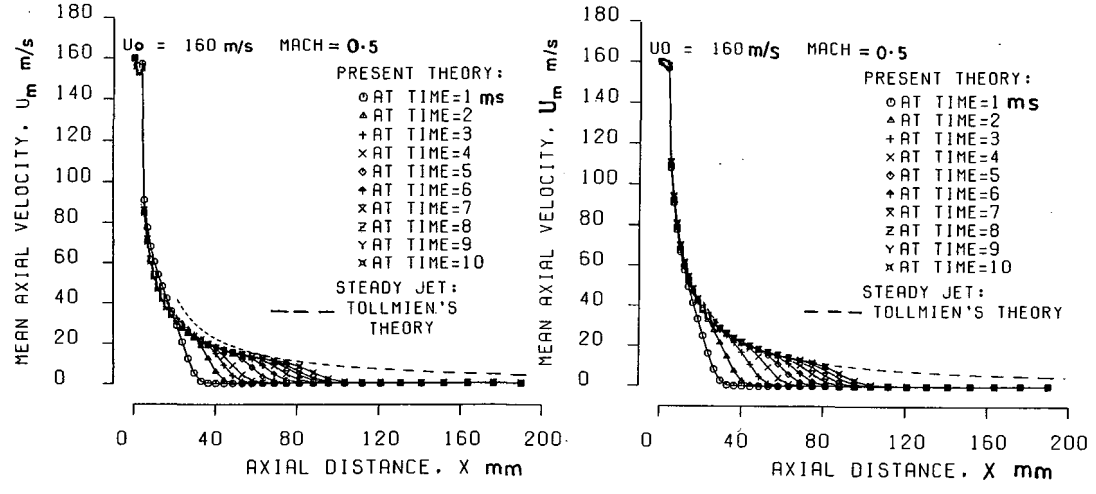

(a) Compressible (b) Incompressible

Fig.3 Histories of axial profiles of mean axial velocity on jet axis

In Fig.3 is shown typical histories of axial profiles of the mean axial velocity U_m as predicted independently by the compressible and incompressible flow solution approaches at several locations on the jet axis for the air jet with initial velocity, Uo =160 m/s. The temporal development of unsteady and steady parts of the transient jet is exhibited more clearly here in that the locations identifying the end of the steady rear parts and the beginning of the unsteady frontal parts of the transient jet are easily seen as the point where these velocity profiles leave the curve profile of the steady jet. Tollmien's steady incompressible jet solution at a divergence factor of 11.8[1,2] is plotted here mainly for two reasons. Firstly, for clarity of result presentation, it serves as a common reference against which compressible and incompressible flow solutions are compared and secondly for checking the accuracy of the present predictions not only in the steady part of the transient jet but also that of both the present transient and quasi-steady jet solutions since it is noted that the steady state numerical solution is obtained by calculation the unsteady flow problem over adequately long time periods. In Tollmien's solution which is well supported by experimental data from many sources[1,2], the Prandtl mixing length hypothesis was used to estimate eddy viscosity, μ_t. Indeed global trends of the present predictions by both compressible and incompressible flow solution approaches compare reasonably with Tollmien's solution particularly in the fully developed downstream main region.

However, in the transition region the compressible flow solution is lower than that of the incompressible flow solution by a maximum of about 8 % at x =24 mm from the jet initiation plane(nozzle). Temporal jet penetration may be estimated from velocity profiles shown in Fig.3 if the velocity of surrounding air pushed ahead of the jet tip is taken into consideration because the pushed air velocity is also part of the velocity profile in the unsteady front part of the jets and the jet tip lies at some location on the jet axis where the axial velocity decays to almost zero. It is seen from Fig.3 that both the compressible and incompressible flow solution approaches predict approximate temporal jet tip penetrations and axial lengths of the steady rear as well as unsteady front parts of the transient jet to almost same degree of accuracy at times, t greater than 2 ms after jet initiation. It is also seen that the axial length of the unsteady front part decreases with time from a maximum of about 50 % of the

approximate jet penetration at time t =1 ms to about 30 % at time 10 ms.

In Fig.4 is shown temporal radial distributions of the axial velocity in the steady rear parts of the transient jet as predicted by the compressible and incompressible flow solution methods at different cross sections. Here, the velocity is normalised by the respective jet

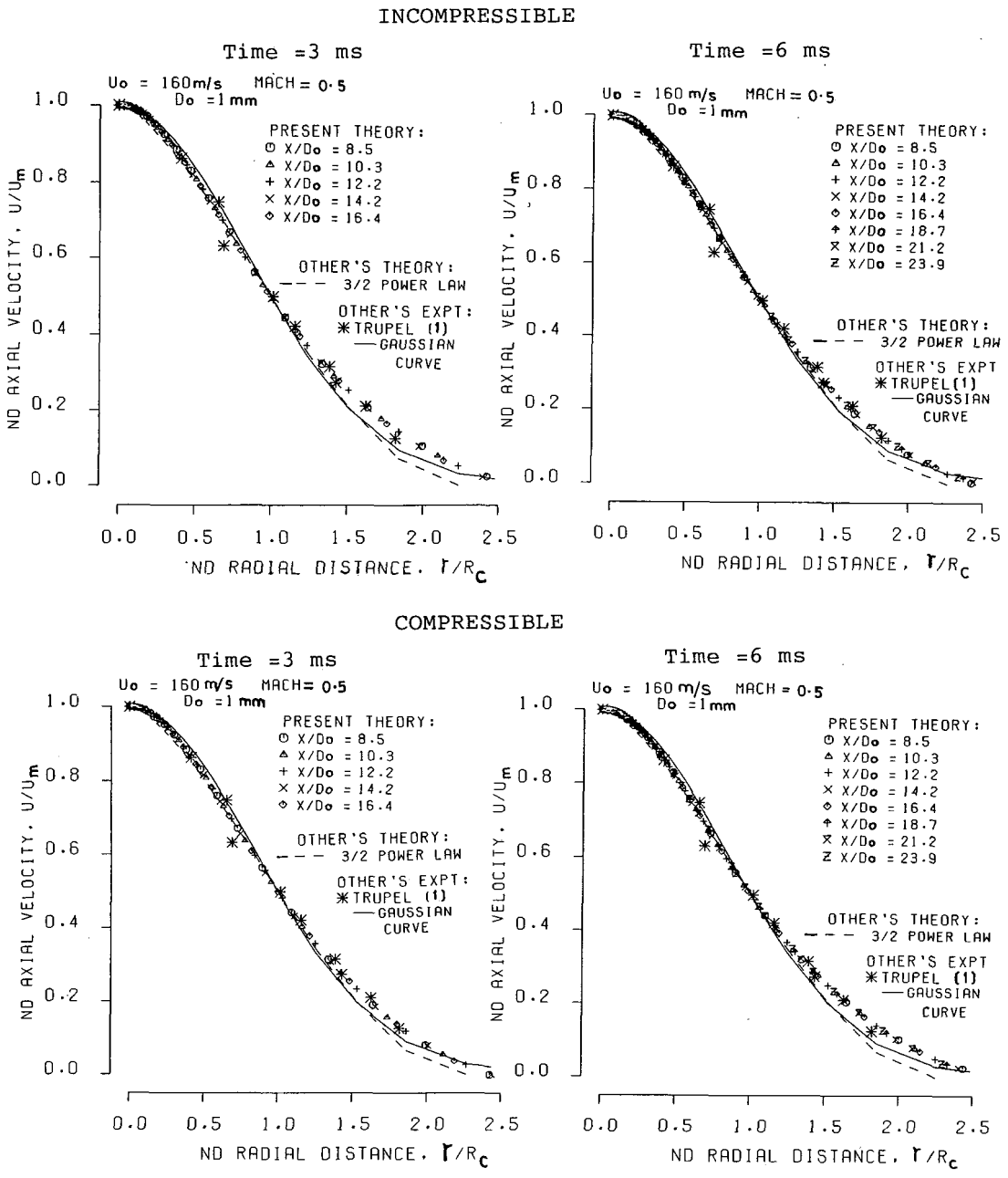

Fig.4 Radial distributions of axial velocity

axis velocity, U_m of the cross section obtained from predictions in Fig.3 while r is normalised by the radial distance R_c at which the axial velocity of the cross section is one-half of U_m and the inner turbulent core are located. Temporal values of R_c which represent the jet radial spread were evaluated from predicted axial velocity fields by interpolation and found to increase linearly with the axial distance at an approximate uniform rate, $R_c = 0.103x$ at all times, $2 \leqq t \leqq 10$ ms in the fully developed region. Since predictions from both methods very closely follow the Gaussian and 3/2 power law curves which represent experimental measurement from many sources[1,10], predictions of radial distributions of the axial velocity by the compressible and incompressible flow approaches are almost identical. Both predictions indicate the similarity and self-preserving nature of the jets in the steady rear parts of transient jets shown by the collapsing of all velocity profiles at different jet cross sections like those shown in Fig.9(a) for the predicted steady jet into a single unique curve. In the steady part of the transient jet, this same property is exhibited at different times after jet initiation. The predicted axial velocity fields may be used for evaluating entrainment by numerical integration.

Transient radial distributions of the radial velocity in steady rear parts of the transient jet as predicted by the compressible and incompressible flow solution approaches are shown in Fig.5. Here, A in the non-dimensional radial velocity and radial distance definitions has a value of 0.78 which is a quotient of a constant, a =0.071 and slope of the half U_m velocity ray of about 0.091[1,2]. Predictions of global trends by both approaches fit Tollmien's prediction fairly well particularly in the inner turbulent core, $r \leqq R_c$ although prediction by the incompressible flow approach is not as good outside this core. This discrepancy is possibly due to non-turbulent flow, complex recirculatory and considerable entrainment flow occurring in the transition and viscous superlayer as well as in the unsteady jet boundary interface region. Like in the case of radial distribution of axial velocity, the similarity and self-preserving properties of even transient jets are exhibited in the steady rear parts of the transient jets at all times by the collapsing of all dimensional velocity profiles at different cross sections as typically shown in Fig.9(b) for the predicted steady jet into a single unique curve with apparent maxima and minima points.

The minima point located at coordinates values (3.57,-0.32) in Fig.5 is the approximate location of the jet outer boundary where the entrainment velocity, V_e occurs at all cross sections. At all cross sections in the steady rear part of the transient jets, present predictions show that the normalized radial location of this minima point does not vary with time which again indicates that the

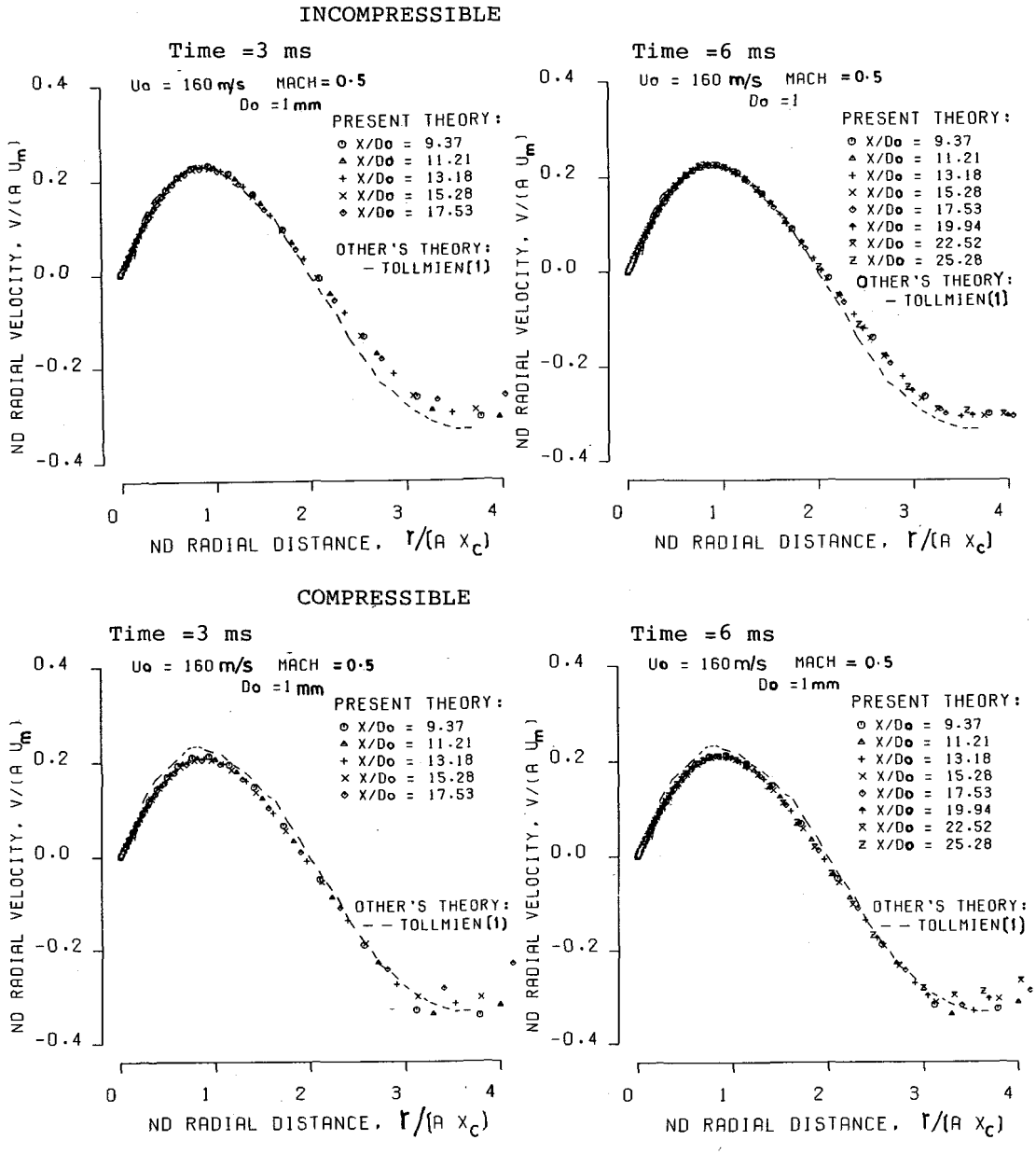

Fig.5 Transient radial distributions of radial Velocity

radial spread of the steady part of the is uniform with time. With the value of A = 0.78, the radial location, R_m of the jet outer boundary may be estimated from the constancy of the normalized radial distance, $R_m/(AR_c)$ = 3.57 as R_m = 2.78R_c while the constancy of $V_e/(AU_m)$=-0.32 is used to derive the entrainment velocity, V_e near or at the minima points which locate the approximate location of the jet outer boundary as V_e = 0.249U_m . Thus knowledge of these coordinate values from present prediction results, R_c obtained by radial interpolation of predicted axial velocity fields and jet axis velocities, U_m from Fig.3 then gives all entrainment velocities and their radial locations from which V_e-based entrainment of the surrounding air has been estimated and found to vary linearly with the axial distance according to the relation, Q_x/Q_o = 0.3x for the steady jet. This entrainment variation is almost identical to the U-based entrainment distribution determined from the predicted axial velocity fields by numerical integration. Here, Q_o and Q_x are the mass flow rates at the nozzle exit and any cross section at axial distance x respectively.

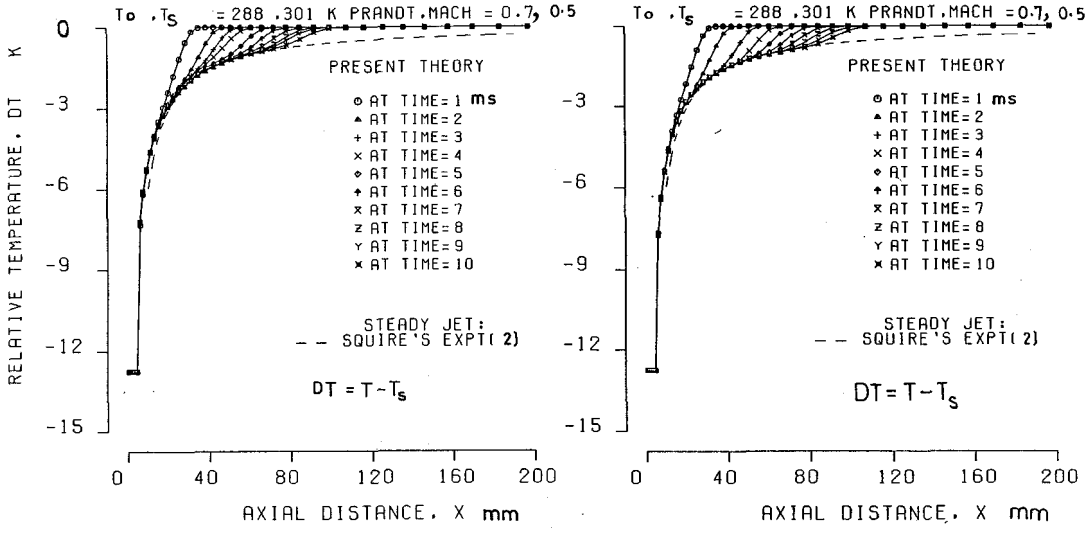

(a) Compressible (b) Incompressible

Fig.6 Histories of axial profiles of relative temperature on jet axis

Temporal axial profiles of relative temperature, DT =T-T_s as predicted by the two solution methods on the jet axis are shown in Fig.6 where Squire's semi-empirical law[2] for jet axis temperature for the steady jet is also plotted as common reference for comparing predictions by the two methods. Here, T_s is the surrounding air

temperature assumed to be same as room temperature and once again solutions by the two methods particularly the global trends of variations in the main region are very nearly identical as they both fit Squire's law closely. The trends of temporal and spatial variation of temperature on jet axis very nearly conform to those of axial velocity given in Fig.3 which may be expected since they are both solved by the same general property transport equation (1) and the present predictions indicate that approximate jet tip penetration indicated by these temperature profiles would reasonably accurate as well. It is also worthy noting the similarity of the predicted axial velocity in the unsteady front parts of the transient jets. When these are normalized as shown in Fig.7, they appear to collapse into one single curve represented by the 3/2 power law;

$$u/u_1 = (1-\{(x-x_1)/(x_0-x_1)\}^{3/2})^2 \qquad (2)$$

where temporal velocity, u_1 and distances x, x_1, x_0 are as shown on the insert. The radial distribution of turbulence intensity in the quasi-steady jet as predicted using the incompressible flow assumption for Uo =160 m/s is shown in Fig.8. The prediction is near to measurement by Corrsin[2] in the inner turbulent core, but higher further outward although the decay trend is similar to measurement by

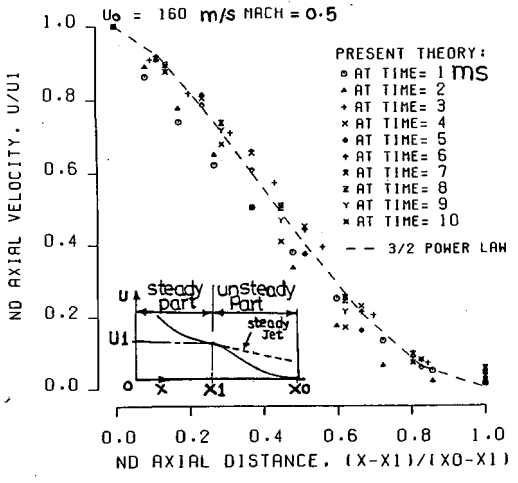

Fig.7 Axial velocity on jet axis in the unsteady front part

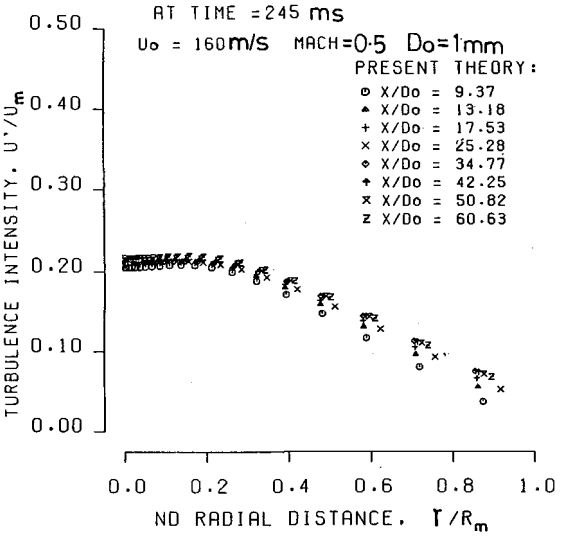

Fig.8 Radial profiles of turbulence intensity

Corrsin. The turbulence velocity, u' is determined from the predicted turbulent kinetic energy using the local isotropy of turbulence assumption[2]. It is maximum near the jet axis at about the same location where the maximum energy dissipation and maximum shear stress occur.

Typical radial distributions of mean axial velocity across several cross sections for the quasi-steady jet at Uo =160 m/s, time =245 ms as predicted using the incompressible flow assumption are shown in Fig.9(a). Again the predicted curves at almost all cross sections in the steady rear part seem similar in shape. The radial distance at which the axial velocity becomes zero roughly locates the jet outermost boundary and so the approximate radial thickness characterising the jet spread. Figure 9(b) shows typical radial distributions of predicted radial velocity across some cross sections of the quasi-steady jet at Uo =160 m/s. These profiles which are also similar in the steady rear parts have a more complicated shape because at each cross section, there exists both positive and negative maxima radial velocities whose magnitudes decrease with the axial distance, x from the injector. Furthermore, radial location of the maximum negative radial velocities increase with the axial distance.

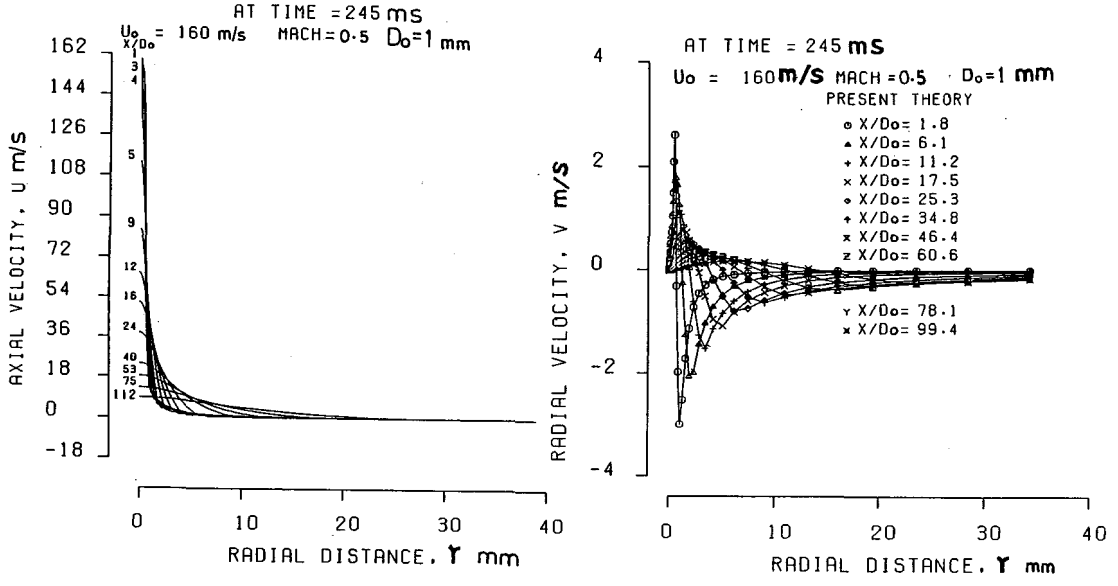

(a) Axial velocity profiles (b) Radial velocity profiles

Fig.9 Axial and radial velocities in the steady jet as predicted using the incompressible flow assumption

It is noted that negative and positive radial velocities represent radial motion towards and away from the jet axis respectively. When compared with the jet spread from radial profiles of predicted axial velocity like those in Fig.9(a), it is worthy noting that the radial location of these predicted maximum negative radial velocities is also the approximate radial location of the jet outermost boundary in the steady rear part of the jet and therefore the maximum negative radial velocities are the approximate entrainment velocities, V_e at the minima points exhibited in Fig.5. The jet spread can therefore also be characterized by the radial locations of the maximum negative radial velocities.

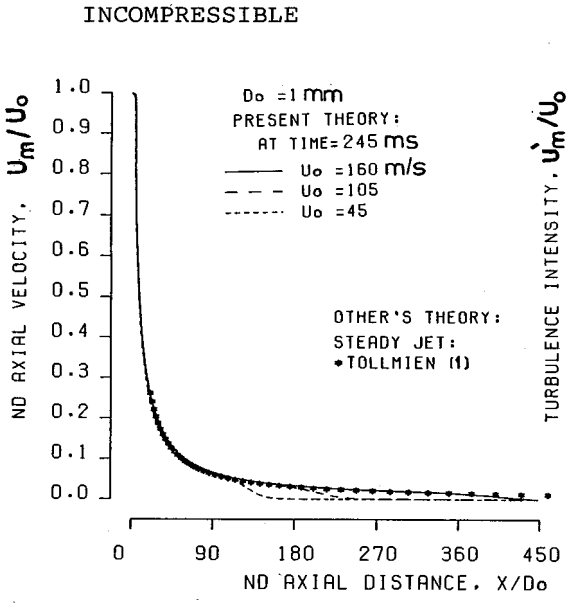

Fig.10 Axial velocity on jet axis of the quasi-steady jet.

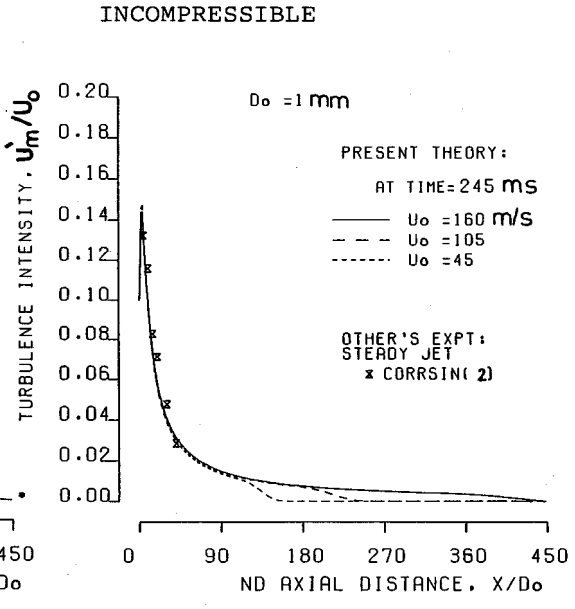

Fig.11. Turbulence intensity on the jet axis of quasi-Steady jet

In Fig.10 is shown axial distribution of the mean axial velocity on the jet axis for all quasi-steady jets as predicted using the incompressible flow assumption. Again in non-dimensional form the velocities are represented by a single curve except in the unsteady front part. Finally, axial distribution of the relative turbulence intensity for all quasi-steady jets as predicted assuming incompressible flow is shown in Fig.11. The turbulence intensities which are determined from the predicted turbulence kinetic energy

using local isotropy of turbulence[2] also collapse into a single curve and vary in a similar way that mean axial velocities upon which they are superimposed vary as shown in Fig.10.

4. CONCLUSIONS

(1) Some seemingly compressible subsonic, high speed free jets discharging into same surrounding gas under atmospheric conditions may be predicted with reasonable accuracy using the incompressible flow assumption. The present calculation results seem to indicate that the compressibility represented by divergence terms in source terms of momentum and turbulence energy dissipation rate equations has negligible effect in solution of some jet flows.

(2) The consistency with which the k-ε has predicted similar turbulent air jet flows at substantially different initial velocities, Uo over short and long calculation times, in transient and steady jets using different time steps and different grid spacings with reasonable accuracy indicates that the k-ε model may be deemed quite reliable and so the Prandtl mixing length hypothesis used by Tollmien.

(3) Present predictions show that the similarity and self-preserving properties of radial distributions of axial and radial velocities as well as temperature which are usually associated with steady jets are also exhibited in the steady rear parts of the transient jets.

REFERENCES

1.Abramovich,G.N.,"The Theory of Turbulent Jets",(1963),MIT.
2.Pai,S-I., "Fluid Dynamics of Jets",(1954),Van Nostran.
3.Kumar,K.L.,"Eng.Fluid Mech.",(1980),Eurasia.
4.Anderson,A.A.et al.,"Comp.Fluid Mech.& Heat Transfer",(1985), McGrawHill.
5.Nsunge,F.C. et al., Numerical Calculation of a Transient, Methane Gas Jet Discharging into Quiscent Atmosphere at Mach One, Memoirs of the Faculty of Eng., Okayama University,Vol.25,No.2(1991).
6.Launder,B.E.et al.,Comp.Methods Appl.Mech.Eng.,Vol.3,(1974),p.269.
7.Launder,B.E.et al.,"Math.Turb.Models",(1972),Academic.
8.Patankar,S.V.,"Num.Heat Transfer & Fluid Flow",(1980),McGrawHill.
9.Witze,P.O.,AIAA J.,Vol.21,No.2(1983),p.308.
10.Rajaratnum,N.,"Turbulent Jets",(1976),Elsevier.